ARTICLES

Journal of Semiconductors
(2020) 41, 042601
doi: 10.1088/1674-4926/41/4/042601

Tubular/helical architecture construction based on rolled-up AlN nanomembranes and resonance as optical microcavity

Jinyu Yang[1], Yang Wang[1], Lu Wang[1], Ziao Tian[2, †], Zengfeng Di[2], and Yongfeng Mei[1, †]

[1]Department of Material Science, Fudan University, Shanghai 200433, China

[2]Shanghai Institute of Microsystem and Information Technology, Chinese Academy of Sciences, Shanghai 20050, China

Abstract: Aluminum nitride (AlN) has attracted a great amount of interest due to the fact that these group III–V semiconductors present direct band gap behavior and are compatible with current micro-electro-mechanical systems. In this work, three dimensional (3D) AlN architectures including tubes and helices were constructed by rolling up AlN nanomembranes grown on a silicon-on-insulator wafer via magnetron sputtering. The properties of the AlN membrane were characterized through transmission electron microscopy and X-ray diffraction. The thickness of AlN nanomembranes could be tuned via the RIE thinning method, and thus micro-tubes with different diameters were fabricated. The intrinsic strain in AlN membranes was investigated via micro-Raman spectroscopy, which agrees well with theory prediction. Whispering gallery mode was observed in AlN tubular optical microcavity in photoluminescence spectrum. A postprocess involving atomic layer deposition and R6G immersion were employed on as-fabricated AlN tubes to promote the *Q*-factor. The AlN tubular micro-resonators could offer a novel design route for Si-based integrated light sources. In addition, the rolled-up technology paves a new way for AlN 3D structure fabrication, which is promising for AlN application in MEMS and photonics fields.

Key words: AlN nanomembranes; rolled-up technology; helices; optical microcavity

Citation: J Y Yang, Y Wang, L Wang, Z A Tian, Z F Di, and Y F Mei, Tubular/helical architecture construction based on rolled-up AlN nanomembranes and resonance as optical microcavity[J]. *J. Semicond.*, 2020, 41(4), 042601. http://doi.org/10.1088/1674-4926/41/4/042601

1. Introduction

Aluminum-nitride (AlN) is an interesting group III–V semiconductor, which presents direct band gap (around 6.2 eV), high thermostability, good piezoelectricity and high chemical stability[1–4]. These excellent properties enable AlN to be an ideal candidate in electrical circuit switches[5], linear photonic circuits, and optical combs[6, 7]. Whispering gallery modes (WGMs), capable of strong light confinement, were utilized in AlN photonic applications ranging from the opto-mechanics[6] to quantum dots[8]. The geometries for supporting WGMs with AlN materials involve micro-rings and microdisks, most of which were limited to two dimensions because of the obstacle in separating AlN nanomembranes (NMs) and substrates. Actually, apart from these structures, various geometries could be applied in WGMs, such as microtubes, micro-bottles, and microspheres[9]. Among them, tubular optical microcavities offer the unique capability of on-chip integration and fluidic handing for analysis besides excellent characteristics of optical microcavities[10], and are considered as a promising geometry for supporting WGMs with AlN materials.

Tubular optical microcavities can be fabricated through rolling-up nanotechnology[11], which is an effective method implemented to construct various 3D structures. This technology was mainly employed on NMs due to the low bending stiffness, and the NM is firstly patterned and then rolled-up into different architectures according to the strain gradient in the membrane[12]. Various 3D structures and corresponding parameters could be precisely tuned by changing two dimensional patterns[13]. For example, tubes with different diameters could be obtained from a different scale of planar circle sheets. Up to now, various devices fabricated from this methodology have been widely employed in phonics[14], electronics[15], integrated sensing[16], and energy storage[17], which would also have great potential in the fabrication of AlN microtubes.

In this work, two typical 3D structures including tubes and helices based on AlN NMs were constructed and WGMs in AlN microtubes were demonstrated and optimized. The good-quality AlN NMs were certified by the microstructural characterization involving the crystallinity and the lattice constant of AlN. Based on the decreased flexural rigidity of AlN NMs after thinning the membrane, the NMs self-assembly transformed into 3D structures via rolled-up nanotechnology. Tubes with various diameters were constructed by controlling the thickness of NMs, and the strain variation before and after the rolling-up process were characterized by a micro-Raman device, which corresponded to the theoretical predication. The WGMs mode was also observed in AlN-based optical microcavities by photoluminescence spectrum. Postprocesses, including atomic layer deposition and R6G immersion, were employed on as-fabricated AlN tubes to promote the quality factor (*Q*-factor).

2. Experimental details

2.1. Growth and characterization of AlN NMs

In this work, the AlN NMs were grown on the Si-on-insulat-

Correspondence to: Z A Tian, zatian@mail.sim.ac.cn; Y F Mei, yfm@fudan.edu.cn

Received 4 SEPTEMBER 2019; Revised 30 OCTOBER 2019.

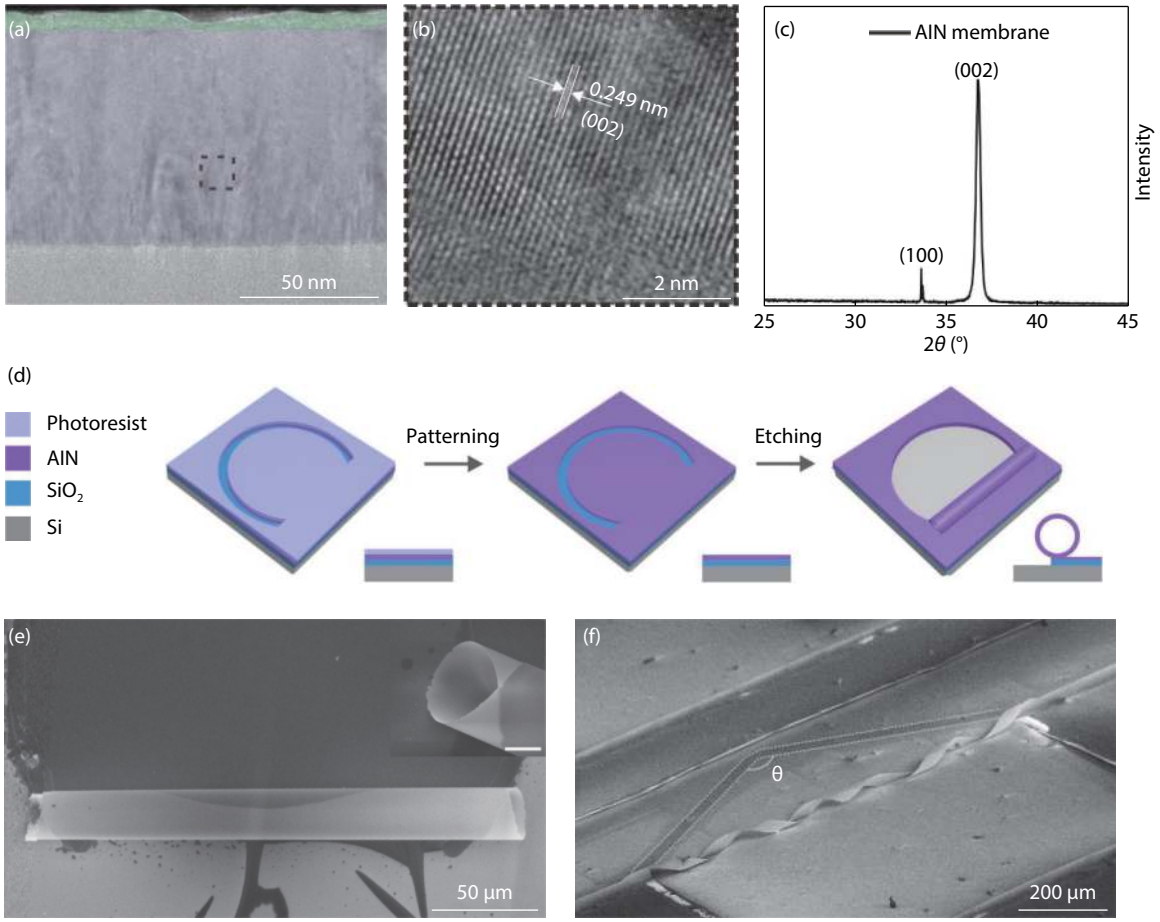

Fig. 1. (Color online) (a) TEM images from the cross section of an aluminum nitride nanomembrane. (b) High resolution TEM image of the AlN component in the nanomembrane. (c) X-ray diffraction pattern of the AlN component. (d) Schematic diagram of the fabrication process using rolled up technology. (e) SEM image of rolled-up tubular structures. inset: the cross-section of the tube (scale bar = 10 μm). (f) SEM image of rolled-up two helices with opposite direction.

or wafer (SOI wafer, with 1 μm SiO_2 top layer) via magnetron sputtering with a nominal thickness of 80 nm provided by Prefab company. The as-grown AlN NMs were then cleaned by ultra-sonication in acetone, ethanol and deionized water for 5 min. After cleaning, the microstructure and element mapping of AlN were characterized by transmission electron microscopy (TEM, FEI TECNAI G2 S-TWIN F20). Before the characterization by TEM, the sample preparation was conducted via focused ion beam (FIB, FEI Helios NanoLab 600). The surface morphology was characterized by atomic force microscope (AFM, BRUKER Dimension Icon). The crystallinity information was given by an X-Ray diffraction device (XRD, BRUKER D8A Advance).

2.2. Fabrication of AlN 3D structures

The photolithography process is a common method to pattern the NMs in the rolling-up process, the AlN 3D structures in this work were constructed utilizing pre-defined patterns. Firstly, a layer of photoresist (AZ5214) was spin-coated on the cleaned AlN NMs at a speed of 4000 r/min. Then, the plate making machine (Heidelberg Upg501) was utilized to create pre-defined patterns on the AlN NMs. The exposure photoresist and the AlN layer downward could be removed by the developing liquid (TMAH, from RuiHong Inc.) simultaneously. Finally, the patterned AlN NMs were rinsed in ethanol to remove the photoresist.

After patterning of AlN NMs, the sample was immersed in a 40% HF solution to selectively remove the sacrificial layer (SiO_2). During the etching process, the top AlN layer released and detached from the substrate. The released NMs then self-assembly roll-up into different 3D structures according to pre-defined patterns and the intrinsic strain in the membrane.

2.3. Thinning process of AlN membrane

Inductively coupled plasma-reactive ion etching (ICP-RIE) was employed to thin the AlN membrane, the parameters used in this work were: 25 sccm total gas flow (20 sccm BCl_3, 5 sccm Ar for stabilization), 20 °C electrode temperature, 30–60 s etching time, 20 mT total pressure, 1000 W ICP power, and a dc-bias of 250 ± 10 V.

2.4. Characterization of AlN microcavities

The morphological property of the as-fabricated AlN structures were characterized via scanning electron microscopy (SEM, JEOL JSM-6701F). Additionally, the micro-Raman scattering spectroscopy (Horiba JY HR-800) with the 532 nm laser as the excitation source was utilized to analyze the strain distribution and optical resonances in AlN microcavities.

3. Results and discussion

Fig. 1(a) shows the TEM image of AlN NMs, including three layers: AlN layer with thickness of 80 nm, SiO_2 layer

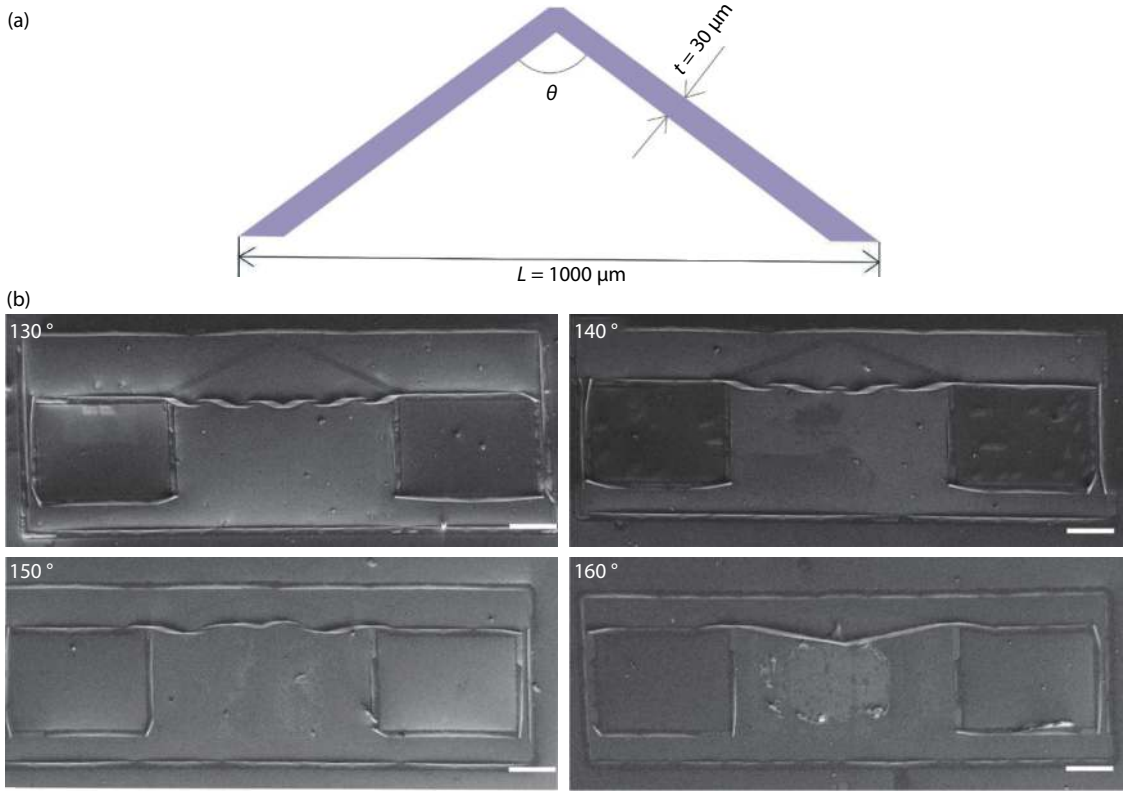

Fig. 2. (Color online) (a) Schematic diagram of V-shaped pattern. (b) SEM images of AlN helices structures fabricated from V-shaped patterns with different angles of 130°,140°,150°,160° (scale bar = 200 μm).

with thickness of 1 μm, and Si layer (not shown in Fig. 1(a)). As well, another layer with thickness of 5 μm, showing amorphous microstructure, was observed above the AlN layer (the green region in Fig. 1(a)). We concluded that it is the oxidation of AlN because condensed O element distribution was confirmed in the layer according to element mapping results (shown in Fig. S1). Fig. 1(b) shows the polycrystalline structure and the main growth direction of AlN NMs with high resolution TEM (HRTEM), the lattice constant of 0.249 nm is corresponding to the (002) plane. XRD pattern of polycrystalline AlN is given in Fig. 1(c). Two peaks near 33.22° and 36.04° could be attributed to (100) and (002) planes of AlN, respectively. The surface morphology of AlN NMs was characterized by atomic force microscope (AFM), as shown in Fig. S2. Columnar structures with pointed tips, or cone structures are in accordance with morphology results in previous work on N-polar AlN[5, 18].

Fig. 1(d) shows the fabrication process of AlN tubular structures. Photolithography was used to pattern the AlN NMs. Different from other materials which need another step to create the etching window on the NMs[13, 19], AlN NMs with N-polar growth direction could react with the developing solution directly[5], by which etching window was formed after the developing process. The patterned AlN NMs were then submerged into HF solution to selectively remove the SiO_2 sacrificial layer. During the HF etching process, the AlN layer would detach from the substrate and self-assembly roll-up into tubular geometry structures. The SEM diagram of AlN tube is given in Fig. 1(e). Starting from circle patterns, AlN tubes with diameters of 20–25 μm was constructed. The inset reveals that the cross section of the tube is symmetrical and uniform.

For AlN polycrystalline membranes with isotropic strain, the rolled-up structures are mainly decided by pre-defined pattern and strain gradient. In this work, two helices of opposite chirality were constructed from V-shaped patterns (marked as the grey dotted lines in Fig. 1(f)). The rolling-up direction of two stripes present competitive behavior, thus this kind of pattern has excellent controllability on helices formation. Moreover, for V-shaped patterns with constant length and width, the helices pitch and the number of turns could be tuned through the angle θ between two stripes (marked as the grey curve in Fig. 1(f)). The statistical results are given in Table 1 (the SEM images of different helices are shown in Fig. 2).

Table 1. Statistical results of different helices.

θ (°)	130	140	150	160
Pitch (μm)	200	250	333.3	>1000
Number of turns	2.5	2	1.5	< 0.5

The pitch increases and the number of turns decreases with increasing θ, which can be explained by limit hypothesis. When θ is limited to zero, two stripes overlap and the competition disappeared, and they will roll-up into the tube which pitch is 0; when θ is limited to 180°, two separate stripes could be considered as a straight stripe with large pitch. The helices in Fig. 1(f) is constructed from V-shaped pattern with θ of 130°. Actually, AlN with (002) crystal orientation also presents piezoelectricity[20]. Compared with piezoelectrical sensors based on 2D structures like bridges and cantilevers[21, 22], 3D helix structure could response to stimulation from every direction and convert the force signal to electrical signal, which has great potential in wearable device fields.

Two parameters which could control the diameter of

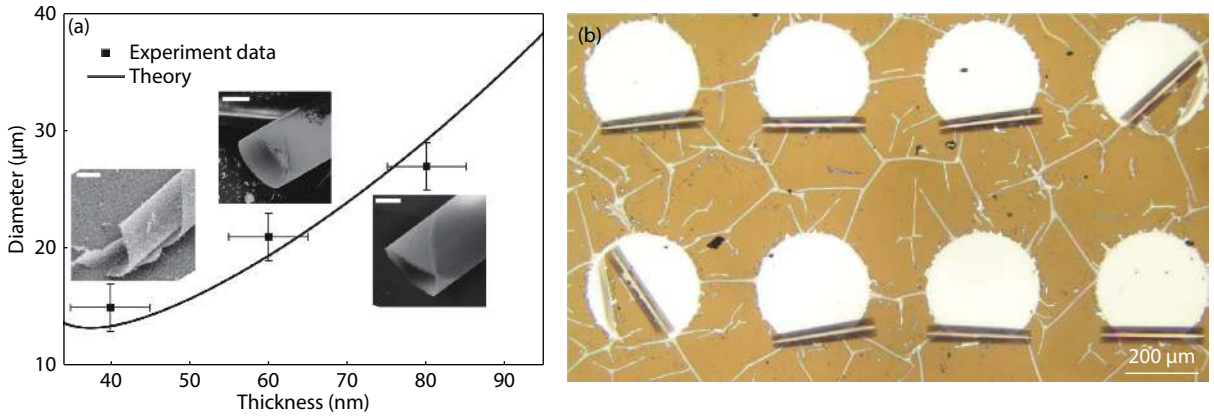

Fig. 3. (Color online) (a) The diameter of a single tube as a function of the AlN membrane thickness after ICP-RIE etching. Insets show corresponding SEM images of microtubes with various diameters (scale bar = 10 μm). (b) Optical microscope image of ordered microtubes array from AlN NMs.

rolled-up tubes are strain gradient and layer thickness[23]. Compared with tuning the strain gradient through postprocess like annealing, thinning membranes is a more facile route with high controllability. The rolling-up behavior of NMs mainly relies on the strain gradient in the membrane originating from the lattice mismatch between substrates and AlN NMs. However, the membrane strain would decrease until zero during the growth procedure[24]. To quantitatively describe the relationship between the membrane thickness and the tube diameter, we divided the AlN membrane into two layers, the relax layer close to surface and the compressive layer close to the substrate (this kind of separation could be explained by AlN rolling behavior, which is always upward)[13]. We assumed that elastic coefficients are equal in the two layers. The diameter of tubes can be calculated by

$$D = \frac{(t_{\text{strain}} + t_{\text{relax}})\left[3(1+m)^2 + (1+m)\left(m^2 + \frac{1}{m}\right)\right]}{3\Delta\varepsilon\,(1+\nu)\,(1+m)^2}, \quad (1)$$

where t_{strain} and t_{relax} are the respective thickness of the compressive and relaxed strain layers, $m = t_{\text{strain}}/t_{\text{relax}}$ is their ratio, $\Delta\varepsilon$ is the strain difference between two layers which could be calculated form Raman shift[25], ν is the Poisson's ratio (0.212)[26], and D is the tube diameter. In our experiment, the ICP-RIE thinning was employed to control the membrane thickness. As shown in Fig. 3(a), the diameter of AlN tube is proportional to the membrane thickness (black spheres), and experiment results present consistent with the theoretical calculation. Starting from circle patterns with thickness of 40 nm, AlN tubes with diameter of 25 μm, length of 300 μm were fabricated and arranged well along a similar direction, as shown in Fig. 3(b).

To clarify the strain gradient in the membrane, micro-Raman device was adopted to AlN NMs before and after the rolling-up process, as shown in Figs. 4(a) and 4(b). Fig. 4(a) shows Raman spectra of as-grown and rolled-up AlN NMs under an excitation laser wavelength of 532 nm. AlN features three Raman peaks in the detectable regime, i.e., the A_1(TO), E_2(high), and A_1(LO). Among them, E_2(high) shows a higher sensitivity to strain variation, thus commonly it is utilized as a symbol to analyze the membrane states[25, 27]. The enlarged view of the Raman spectra is given in Fig. 4(b). Compared with a totally relaxed membrane (the grey dotted line, acquired from previous researches[25]), the E_2(high) peak of as-grown membrane shifted from 656 to 657.78 cm^{-1}, leading to a 1.78 cm^{-1} redshift, which is corresponding to the compressive strain in the membrane[27]. The E_2(high) of rolled-up membrane shifted from 656 to 654.50 cm^{-1}, inducing a 1.5 cm^{-1} blueshift, attributed to the layer close to substrate being stretched after the upward rolling process.

The linear relationship between stress variation and E_2(high) shift has been investigated in previous reports[25], in which researchers endeavored to find a linear coefficient to simplify the membrane stress calculation. Here, we employed ω (cm^{-1}/GPa) to describe this relationship. The equation is as follows.

$$\sigma = \frac{\omega_0 - \omega}{-\Delta\omega}, \quad (2)$$

$\Delta\omega$ is the linear coefficient –2.9 (cm^{-1}/GPa), ω_0 is the E_2(high) peak position in the relaxed membrane and ω is in the stressed state, σ is the intrinsic stress. Combining with the experiments, stress in the as-grown membrane calculated from this equation is –613 MPa (– means the stress in the membrane is compressive). Stress in the rolled-up membrane is +517 MPa (+ means the stress is tensile). Strain could be deduced from stress with Yong's modulus.

Eventually, the optical characterization of AlN microcavities was carried out via photoluminescence (PL) measurements. The result is given in Fig. 4(c) (marked as a blue line), AlN microcavity fabricated from rolling-up technology presented a stable WGM mode in the range of 580–600 nm. Actually, the band gap of AlN is around 6.2 eV, which, in theory, couldn't be excited by 532 nm wavelength laser. However, the impurity introduction couldn't be prohibited totally in the membrane growth process in reality. From the element mapping result (given in Fig. S1), uniform oxygen element distribution was observed in the AlN region, which indicates that defects like oxygen point defects (O_N^+), nitrogen vacancies (V_N), and $V_{Al}^{3-} - 3xO_N^+$ complexes may exist in the AlN film[28, 29]. Moreover, the defects preferred to form or increase during the etching process. Therefore, the PL range was expanded.

The Q-factor could be calculated from the equation

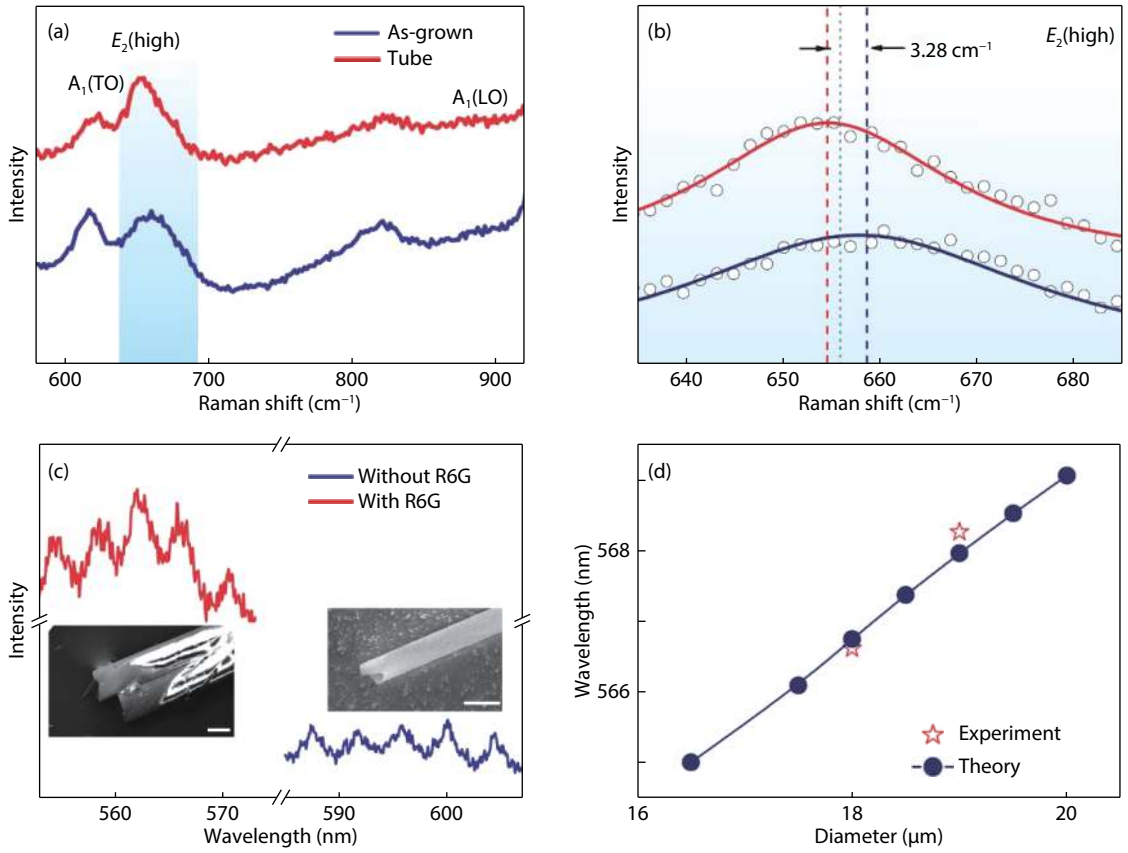

Fig. 4. (Color online) (a) Raman spectra of AlN before and after the rolling-up process. (b) Enlarged view of Raman peak shift. (c) Optical resonance of AlN microcavity before (blue line) and after (red line) the ALD process. Insets show corresponding SEM images of AlN microcavity before (scale bar = 20 μm) and after postprocess (scale bar = 30 μm). (d) Simulated mode positions as a function of tubes with various diameters (blue line and circle symbol). Experimental results showed as red star symbols.

$$Q = \lambda/\Delta\lambda, \tag{3}$$

where λ is the resonant wavelength, $\Delta\lambda$ is the FWHM corresponding to the full width at half maximum of the resonant peak. The calculated result shows the Q-factor of as-fabricated AlN microcavities is around 200, which is at medium level among rolled-up tubular resonators, such as SiO_x/Si (Q < 100), GaN (Q ~ 100), and Y_2O_3/ZrO_2 (Q > 1500)[30]. As the SEM images of the as-fabricated tube show, clear surface roughness could be seen outside the tube, leading to surface scattering and poor light confinement. To improve the light confinement effect and increase the Q-factor, atom layer deposition (ALD) and subsequent submerging into R6G solution were employed as the postprocess. ALD, an effective method which could improve the optical property of tubular microcavities, has been introduced in a previous work[10]. Dense and uniform membranes could be obtained on both the external and the inner side of the tube after ALD. In the current work, AlN tubes were coated by a layer of Al_2O_3 with 50 nm thickness, then immersed into R6G solution. The result is given in Fig. 4(c) (marked as the red line). WGM modes were also observed in the postprocessed microcavity tubes. Compared with as-fabricated microcavities, PL range shifted to shorter wavelength (about 540–570 nm), which is close to the intrinsic emission peak of the dye emitter in R6G at around 550 nm. The Q-factor is used to evaluate the photon lifetime in the optical microcavity, which is mainly affected by effective refractive index n_{eff}[31]. The Q-factor of tubular optical microcavity before and after the postprocess was improved from 193 to 291 (m = 146, λ = 595 nm). The main reason for this is the effective refractive index n_{eff} increment caused by the wall thickening. According to the n_{eff} formula,

$$n_{eff} = [1 + i\sigma/\omega\varepsilon_0\Delta]^{1/2}, \tag{4}$$

where Δ is the wall thickness, σ is the material conductivity, ε_0 is the vacuum dielectric constant and ω is the angular frequency. The n_{eff} could be divided into a real part and an imaginary part i, and the imaginary part was used to evaluate the light loss. With Δ increased, the imaginary part decreased and the light loss in the propogation process will reduce. In other words, the Q factor increased. Lin[10] also confirmed this illustration in her work.

Tubes with different diameters have been fabricated in the last section, then the resonance peak shifts caused by the diameter variation was further investigated. Simulation by finite element methods is given in Fig. 4(d) (blue line and circle symbol). For a given mode, the resonance shifted to longer wavelength with increasing the diameter of tube. Experiments result (red star symbols in Fig. 4(d)) is consistent with the simulation.

4. Conclusion

In conclusion, AlN tubular micro-resonator were fabricated by rolling up AlN NMs grown on SOI. Microstructural characterization demonstrated that the AlN main growth direction is (002). The thickness and the stiffness of AlN NMs were

reduced through ICP-RIE process, the thickness was tuned to 40, 60, and 80 nm respectively, then AlN tubes with different diameters (d = 15, 21, and 29 μm) were fabricated. Stress distributions of the as-grown and the rolled-up AlN membrane were characterized via micro-Raman spectroscopy and specific values of stress were deduced from the Stress–Raman shift formula. The calculation results show that the membrane stress was shifted from –613 to +517 MPa after rolling up process (– means the compressive stress, + means the tensile stress). Micro-Raman measurements showed the resonant behavior of as-fabricated AlN micro-cavities clearly, and the Q-factor reached 193. Postprocess was utilized to improve the Q-factor to 291, which advancement could be explained by tube refractive index increment. Such AlN micro-resonators based on tubular microcavities offer a novel design route for Si-based integrated light source. Moreover, the rolled-up technology provides a new possibility for AlN 3D structures fabrication, which is promising for AlN application in MEMS and photonics fields.

Acknowledgments

This work was supported by the National Natural Science Foundation of China (Nos. 61905270, 51961145108), Natural Science Foundation of Shanghai (19ZR1467100), Science and Technology Commission of Shanghai Municipality (17JC1401700), and the Program of Shanghai Academic Research Leader (19XD1400600).

References

[1] Vurgaftman I, Meyer J R, Ram-Mohan L R. Band parameters for III–V compound semiconductors and their alloys. J Appl Phys, 2001, 89(11), 5815

[2] Li L W, Bando Y, Zhu Y C, et al. Single-crystalline AlN nanotubes with carbon-layer coatings on the outer and inner surfaces via a multiwalled-carbon-nanotube-template-induced route. Adv Mater, 2005, 17(2), 213

[3] Bowen C R, Kim H A, Weaver P M, et al. Piezoelectric and ferroelectric materials and structures for energy harvesting applications. Energy Environ Sci, 2013, 7, 25

[4] Zheng B J, Hu W. Cubic AlN thin film formation on quartz substrate by pulse laser deposition. J Semicond, 2016, 37(6), 063003

[5] Sinha N, Wabiszewski G E, Mahameed R, et al. Piezoelectric aluminum nitride nanoelectromechanical actuators. Appl Phys Lett, 2009, 95(5), 053106

[6] Xiong C, Pernice W H P, Sun X, et al. Aluminum nitride as a new material for chip-scale optomechanics and nonlinear optics. New J Phys, 2012, 14(9), 095014

[7] Longhi S, Feng L. Unidirectional lasing in semiconductor microring lasers at an exceptional point. Photonics Res, 2017, 5(6), B1

[8] Bürger M, Ruth M, Declair S, et al. Whispering gallery modes in zinc-blende AlN microdisks containing non-polar GaN quantum dots. Appl Phys Lett, 2013, 102(8), 081105

[9] Wang J, Zhan T, Huang G, et al. Optical microcavities with tubular geometry: properties and applications. Laser Photonics Rev, 2014, 8(4), 521

[10] Lin X, Fang Y, Zhu L, et al. Self-rolling of oxide nanomembranes and resonance coupling in tubular optical microcavity. Adv Opt Mater, 2016, 4(6), 936

[11] Kipp T, Welsch H, Strelow C, et al. Optical modes in semiconductor microtube ring resonators. Phys Rev Lett, 2006, 96(7), 077403

[12] Huang G, Mei Y. Assembly and self-assembly of nanomembrane materials—from 2D to 3D. Small, 2018, 14(14), 1703665

[13] Tian Z, Zhang L, Fang Y, et al. Deterministic self-rolling of ultrathin nanocrystalline diamond nanomembranes for 3D tubular/helical architecture. Adv Mater, 2017, 29(13), 1604572

[14] Huang G S, Mei Y F, Cavallo F, et al. Fabrication and optical properties of C/β-SiC/Si hybrid rolled-up microtubes. J Appl Phys, 2009, 105, 016103

[15] Yu X, Huang W, Li M, et al. Ultra-small, high-frequency, and substrate-immune microtube inductors transformed from 2D to 3D. Sci Rep, 2015, 5, 9661

[16] Fang Y, Li Xn, Tang S, et al. Temperature-dependent optical resonance in a thin-walled tubular oxide microcavity. Prog Nat Sci Mater, 2017, 27(4), 498

[17] Yan C, Xi W, Si W, et al. Highly conductive and strain-released hybrid multilayer Ge/Ti nanomembranes with enhanced lithium-ion-storage capability. Adv Mater, 2013, 25(4), 539

[18] Kim J, Choi U, Pyeon J, et al. Deep-ultraviolet AlGaN/AlN core-shell multiple quantum wells on AlN nanorods via lithography-free method. Sci Rep, 2018, 8(1), 935

[19] Huang G, Mei Y. Thinning and shaping solid films into functional and integrative nanomembranes. Adv Mater, 2012, 24(19), 2517

[20] Akiyama M, Morofuji Y, Kamohara T, et al. Flexible piezoelectric pressure sensors using oriented aluminum nitride thin films prepared on polyethylene terephthalate films. J Appl Phys, 2006, 1143185

[21] Zhao C, Knisely K E, Colesa D J, et al. Voltage readout from a piezoelectric intracochlear acoustic transducer implanted in a living guinea pig. Sci Rep, 2019, 9, 3711

[22] Ledermann N, Muralt P, Baborowski J, et al. Piezoelectric Pb(Zr_x, Ti_{1-x})O_3 thin film cantilever and bridge acoustic sensors for miniaturized photoacoustic gas detectors. J Micromech Microeng, 2004, 14, 1650

[23] Froeter P, Yu X, Huang W, et al. 3D hierarchical architectures based on self-rolled-up silicon nitride membranes. Nanotechnology, 2013, 24(47), 475301

[24] Dodson B W, Tsao J Y. Relaxation of strained-layer semiconductor structures via plastic flow. Appl Phys Lett, 1987, 51(17), 1325

[25] Trodahl H J, Martin F, Muralt P, et al. Raman spectroscopy of sputtered AlN films: E2 (high) biaxial strain dependence. Appl Phys Lett, 2006, 89(6), 061905

[26] Yonenaga I, Shima T, Sluiter M H F. Nano-indentation hardness and elastic moduli of bulk single-crystal AlN. Jpn J Appl Phys, 2002, 41(7R), 4620

[27] Kuball M, Hayes J M, Prins A D, et al. Raman scattering studies on single-crystalline bulk AlN under high pressures. Appl Phys Lett, 2001, 78(6), 724

[28] Tang Y, Cong H, Li F, et al. Synthesis and photoluminescent property of AlN nanobelt array. Diamond Relat Mater, 2007, 16(3), 537

[29] Cao Y G, Chen X L, Lan Y C, et al. Blue emission and Raman scattering spectrum from AlN nanocrystalline powders. J Cryst Growth, 2000, 213(1/2), 198

[30] Wang J, Song E, Yang C, et al. Fabrication and whispering gallery resonance of self-rolled up gallium nitride microcavities. Thin Solid Films, 2017, 627, 77

[31] Wang J, Zhang T, Huang G, et al. Tubular oxide microcavity with high-indexcontrast walls: Mie scattering theory and 3D confinement of resonant modes. Opt Express, 2012, 20(17), 18555